Hindawi
Geofluids
Volume 2022, Article ID 3320738, 11 pages
https://doi.org/10.1155/2022/3320738

Research Article

Application of the Maximum Sensitivity Principle in the Optimization of Measuring Point Arrangement in Transversely Isotropic Rock Mass Engineering

Yongtao Li[1] **and Zhizeng Zhang**[2]

[1]*School of Construction Engineering, Zhengzhou Shengda University, Zhengzhou 450007, China*
[2]*College of Civil Engineering and Architecture, Zhongyuan University of Technology, Zhengzhou 450007, China*

Correspondence should be addressed to Zhizeng Zhang; zhangzhizeng@163.com

Received 23 March 2022; Revised 2 May 2022; Accepted 6 May 2022; Published 11 June 2022

Academic Editor: Hao Wu

The inverse analysis method based on in situ measurement information provides a new approach to determine the mechanical parameters of rock mass. The accurate on-site monitoring data is the prerequisite and basis for the success of displacement back analysis. To improve the accuracy of requirement parameters, a reasonable layout program should be developed to optimize the layout of the measuring position. In order to study the optimal arrangement of measuring points in anisotropic rock mass, the layout optimization of measuring points around a tunnel in the transversely isotropic rock mass is studied according to the maximum sensitivity criteria. The influence of the spatial location of the measuring points on the measurement of the tunnel deformation is obtained. The results indicate that the measuring point should be arranged close to the extreme point in the direction of the larger principal stress.

1. Introduction

In underground cavern engineering, displacement monitoring, as an effective means to obtain the dynamic changes of rock mass in underground engineering, provides a reliable basis and adjustment direction for the dynamic design, construction, and management of underground engineering. The displacement monitoring results can provide the basis for the modification of supporting structure parameters. It can also be used to analyze the dynamic changes of tunnel surrounding rock and provide safety information for tunnel construction and long-term use. It can provide a basis for the correct selection of excavation methods and support construction time. Wu et al. [1] also determined the crack type and failure mode of the tunnel through numerical simulation based on the field monitoring data. On the basis of on-site monitoring and numerical simulation, Cheng et al. [2] predict the real creep of salt caverns through long-term creep tests, which provides a new idea for monitoring rock mass deformation. Xu et al. [3] proposed a real-time monitoring method and system and established multi-index early warning and damage criteria for roadway deformation failure, including displacement, speed, and acceleration. Wang et al. [4] analyzed the fracture position of the main roof by monitoring the deformation and stress of the surrounding rock of the coal seam and put forward an early warning for the construction. Pan et al. [5, 6] applied the monitoring technology to the rock mass grouting technology and verified it through numerical simulation. The research has guiding significance for the monitoring of broken rock mass. The importance of displacement monitoring in tunnel engineering can be seen.

In addition, accurate on-site monitoring data is the prerequisite and basis for the success of displacement back analysis. Currently, according to the spatial layout principle of measuring points, the following three theoretical systems have been formed: the principle of the maximum displacement [7],

the principle of the maximum sensitivity [8, 9], and the principle of the minimum variance [10, 11]. Kernevez et al. [12] believed that the spatial position of the measuring points was more important than the number of measuring points and there existed a critical number of the measuring point. According to engineering calculation, Sun et al. [13] considered that the influence of increasing the number of the measuring point on the result of back analysis was little. Based on the idea of sensitive displacement components, Yang [14] discussed the accuracy criteria and optimization of the placement of displacement components. Xiang [15–17] proposed the criterion of optimization arrangement for measurement points. Huang [18] used the sensitivity principle to analyze the layout of measuring points in material parameter identification of two-dimensional orthotropic bodies. By constructing the square sum of the difference between the measured displacement and the corresponding displacement calculated by the boundary element as the objective function, Huang [19] used the Levenberg-Marquardt method to iterate the minimization objective function, thereby transforming the parameter identification problem into a minimization objective function. Built on the finite element software ABAQUS, Li et al. [20] conducted a parameter identification algorithm software design and compiled a user unit program that can calculate the sensitivity of the node displacement to the material parameters. Then, the accurate material parameters can be obtained. Zhang [21, 22] analyzed the optimization arrangements for measurement points in transversely isotropic material based on the principle of the maximum displacement. She [23–25] adopted the most perceptive principle to optimize the survey line and carried out engineering back analysis. Zhang et al. [26, 27] used the horizontal stratified anisotropic random field to study the influencing factors of tunnel convergence and proposed a scale factor method considering spatial variability.

In the above research, the research on the optimal layout of measuring points was mostly aimed at isotropic rock mass. With the development of the theory and practice of underground cavern engineering, the importance of rock mass anisotropy is highlighted. However, there were few studies on the optimal layout of measuring points in the displacement back analysis of anisotropic rock mass. There are few studies on the optimal arrangement of measuring points based on the principle of maximum sensitivity. Therefore, based on the maximum sensitivity principle, this paper attempts to study the optimal arrangement of measuring points in a circular tunnel in transversely isotropic rock mass and find out some principles for the arrangement of displacement measuring points. Transversely isotropic rock mass is a special case of anisotropic rock mass. The elastic properties in all directions in a certain plane of the rock are the same, and this surface is called an isotropic surface. However, the mechanical properties in the direction perpendicular to this surface are different. The rock mass with this feature is referred to as the transversely isotropic rock mass.

Based on the principle of maximum sensitivity and the analytical solution of displacement of circular tunnel in transversely isotropic rock mass, the sensitivity criterion of displacement to the radius and angle of measuring point arrangement is theoretically deduced in this study. Combined with engineering examples, numerical simulation is used to analyze the position where the maximum displacement occurs under different stress states, and the theoretical results are verified. The research results can provide a basis for the layout of measuring points in underground engineering.

2. Maximum Sensitivity Criteria

The sensitivity function is as follows:

$$G(x_i) = \frac{\partial F(x)}{\partial x_i}. \tag{1}$$

In Equation (1), $G(x)$ is the objective function, $F(x)$ is the parameter equation of x, and x is the independent variable. The function of $F(x)$ is an increasing function about x when $G(x) > 0$. It is a reducing function about x when $G(x) < 0$. If $G(x) = 0$, slight change of x has no effect on $F(x)$. In engineering, the absolute value of $G(x)$ is usually used to reflect the change degree of $F(x)$ at point x. The greater the absolute value, the greater the sensitivity.

Since the degree of difficulty in inversing the parameters is dependent on the sensitivity of the parameter, the maximum sensitivity criteria are used as the principle of arrangement for measurement points. However, it is applied when the partial derivatives of the model parameters can be easily obtained, or there is more than one parameter to be inversed.

3. Optimization Arrangement for Measurement Points of the Circular Roadway in the Transversely Isotropic Rock Mass

3.1. Sensitivity Analyses of the Angle to Displacement. Figure 1 presents an idealized model for a circular tunnel in transversely isotropic rock mass. The transversely isotropic rock mass means that the rock mass has the same material constant in any direction parallel to the plane, and the material parameters of the parallel and vertical planes are different. The transversely isotropic elastomer has five independent elastic constants, namely, μ, E', μ', and G'.

Zhang [21] deduced the displacement analytical solution of round tunnel as follows:

$$u_r = \frac{p+q}{2}\frac{a^2}{r}\frac{1+\mu}{E} + \frac{p-q}{2}\left[\frac{a^4}{r^3}\frac{1+\mu}{E} - \frac{4a^2}{r}\left(\frac{1}{E} - \frac{\mu'^2}{E'}\right)\right]\cos 2\theta, \tag{2}$$

where u_r is the radial displacement; q and p are the horizontal and vertical initial ground stresses, respectively; E and μ are, respectively, the elastic modulus and Poisson's ratio in the isotropic plane; E' and μ' are the corresponding elastic constants in the direction perpendicular to the isotropic plane; a is the radius of the tunnel; and r and θ are the polar diameter and angle in polar coordinates.

In Equation (2), $u_r > 0$ indicates that the direction of displacement is toward the excavation face, and $u_r < 0$ indicates that the direction is away from the excavation face.

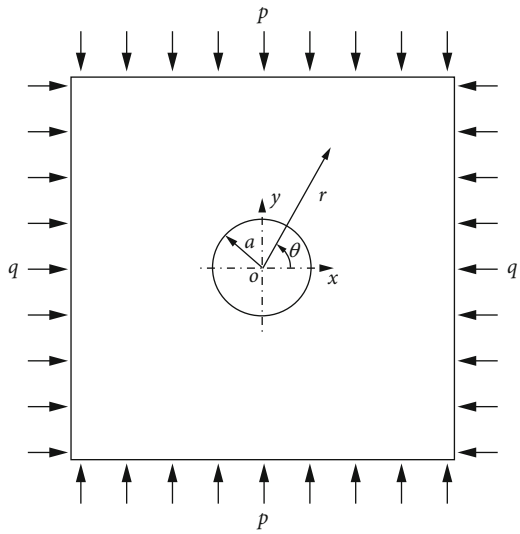

Figure 1: Model for a circular tunnel in transverse isotropy.

Xiang et al. [16] conducted a study on the uniqueness of the back analysis of transversely isotropic rock mass displacements and concluded that p and q are the most identifiable. Therefore, the sensitivity coefficients of radial displacement to the parameters p and q can be obtained, respectively, as follows:

$$\frac{\partial u_r}{\partial p} = \frac{1}{2}\frac{a^2}{r}\frac{1+\mu}{E} + \frac{1}{2}\left[\frac{a^4}{r^3}\frac{1+\mu}{E} - \frac{4a^2}{r}\left(\frac{1}{E} - \frac{\mu'^2}{E'}\right)\right]\cos 2\theta, \tag{3}$$

$$\frac{\partial u_r}{\partial q} = \frac{1}{2}\frac{a^2}{r}\frac{1+\mu}{E} - \frac{1}{2}\left[\frac{a^4}{r^3}\frac{1+\mu}{E} - \frac{4a^2}{r}\left(\frac{1}{E} - \frac{\mu'^2}{E'}\right)\right]\cos 2\theta. \tag{4}$$

The relationship between the parameters is shown in Equation (2):

$$\frac{a^4}{r^3}\frac{1+\mu}{E} - \frac{4a^2}{r}\left(\frac{1}{E} - \frac{\mu'^2}{E'}\right) < 0. \tag{5}$$

According to the maximum sensitivity criteria, the value of the sensitivity coefficients $\partial u_r/\partial p$ and $\partial u_r/\partial q$ can be maximized at the point of $\cos 2\theta = -1$ and $\cos 2\theta = 1$, respectively. Then, the function of θ will lead to $\theta = 90^\circ$ and $\theta = 0^\circ$, respectively.

According to the initial ground stress, the variation of displacement with the angle in three cases would be discussed.

$$p - q = 0. \tag{6}$$

In this case, Equation (2) transforms into

$$u_r = \frac{p+q}{2}\frac{a^2}{r}\frac{1+\mu}{E}. \tag{7}$$

It can be seen from Equation (7) that there is no direct relationship between the displacement and the angle θ, and the displacement is equal in a circle around the origin.

$$p - q > 0. \tag{8}$$

u_r increases with θ during the interval $0^\circ \le 2\theta \le 180^\circ$, and it decreases during the interval $180^\circ \le 2\theta \le 360^\circ$.

Therefore, u_r reaches the maximum value when $\theta = 90^\circ$. The equation is as follows:

$$u_{r\,max} = \frac{p+q}{2}\frac{a^2}{r}\frac{1+\mu}{E} - \frac{p-q}{2}\left[\frac{a^4}{r^3}\frac{1+\mu}{E} - \frac{4a^2}{r}\left(\frac{1}{E} - \frac{\mu'^2}{E'}\right)\right]\cos 2\theta. \tag{9}$$

u_r reaches the minimum value when $\theta = 0^\circ$. The equation is as follows:

$$u_{r\,min} = \frac{p+q}{2}\frac{a^2}{r}\frac{1+\mu}{E} + \frac{p-q}{2}\left[\frac{a^4}{r^3}\frac{1+\mu}{E} - \frac{4a^2}{r}\left(\frac{1}{E} - \frac{\mu'^2}{E'}\right)\right]\cos 2\theta, \quad p - q < 0. \tag{10}$$

u_r decreases with θ during the interval $0^\circ \le 2\theta \le 180^\circ$, and it increases during the interval $180^\circ \le 2\theta \le 360^\circ$.

Therefore, u_r reaches the maximum value when $\theta = 0^\circ$. The equation is as follows:

$$u_{r\,max} = \frac{p+q}{2}\frac{a^2}{r}\frac{1+\mu}{E} + \frac{p-q}{2}\left[\frac{a^4}{r^3}\frac{1+\mu}{E} - \frac{4a^2}{r}\left(\frac{1}{E} - \frac{\mu'^2}{E'}\right)\right]\cos 2\theta. \tag{11}$$

u_r reaches the minimum value when $\theta = 90^\circ$. The equation is as follows:

$$u_{r\,min} = \frac{p+q}{2}\frac{a^2}{r}\frac{1+\mu}{E} - \frac{p-q}{2}\left[\frac{a^4}{r^3}\frac{1+\mu}{E} - \frac{4a^2}{r}\left(\frac{1}{E} - \frac{\mu'^2}{E'}\right)\right]\cos 2\theta. \tag{12}$$

From the above analysis, it can be seen that the maximum displacement always occurs in the direction of larger initial stress, and the smallest displacement always occurs in the direction of smaller initial stress. However, according to Equation (3) and Equation (4), the arrangement of measuring points in the two principal stress directions is most beneficial for the inversion of parameters.

3.2. Sensitivity Analyses of the Radius to Displacement. The sensitivity function of the radius to displacement can be obtained from calculating the partial derivative. The sensitivity function is as follows:

$$\frac{\partial u_r}{\partial r} = -\frac{p+q}{2}\frac{a^2}{r^2}\frac{1+\mu}{E} + \frac{p-q}{2}\left[\frac{-3a^4}{r^4}\frac{1+\mu}{E} + \frac{4a^2}{r^2}\left(\frac{1}{E} - \frac{\mu'2}{E'}\right)\right]\cos 2\theta = \frac{a^2}{r^2}\left\{-\frac{p+q}{2}\frac{1+\mu}{E} + \frac{p-q}{2}\left[\frac{-3a^2}{r^2}\frac{1+\mu}{E} + 4\left(\frac{1}{E} - \frac{\mu'2}{E'}\right)\right]\cos 2\theta\right\},$$

$$\frac{\partial^2 u_r}{\partial r^2} = -\frac{p+q}{2}\frac{-2a^2}{r^3}\frac{1+\mu}{E} + \frac{p-q}{2}\left[\frac{12a^4}{r^5}\frac{1+\mu}{E} + \frac{-8a^2}{r^3}\left(\frac{1}{E} - \frac{\mu'2}{E'}\right)\right]\cos 2\theta = \frac{a^2}{r^3}\left\{(p+q)\frac{1+\mu}{E} + \frac{p-q}{2}\left[\frac{12a^2}{r^2}\frac{1+\mu}{E} - 8\left(\frac{1}{E} - \frac{\mu'2}{E'}\right)\right]\cos 2\theta\right\}. \tag{13}$$

Let $\partial^2 u_r/\partial r^2 = 0$; then, the following formula can be obtained:

$$(p+q)\frac{1+\mu}{E} + \frac{p-q}{2}\left[\frac{12a^2}{r^2}\frac{1+\mu}{E} - 8\left(\frac{1}{E} - \frac{\mu'^2}{E'}\right)\right]\cos 2\theta = 0. \tag{14}$$

The extreme value can be obtained as follows:

$$r_{\text{Extreme}} = \sqrt{\frac{6}{\left[4\left((1/E) - \left(\mu'^2/E'\right)\right)/((1+\mu)/E)\right] - [(p+q)/(p-q)\cos 2\theta]}}\cdot a. \tag{15}$$

When the equation $(p+q)/(p-q)\cos 2\theta = [4((1/E) - (\mu'^2/E'))/((1+\mu)/E)] - 6$ is set up, $r_{\text{extreme}} = a$. The sensitivity at the cave wall reaches the maximum value.

When the equation $(p+q)/(p-q)\cos 2\theta > [4((1/E) - (\mu'^2/E'))/((1+\mu)/E)] - 6$ is set up, $r_{\text{extreme}} > a$. Then, there is a maximum sensitivity at the extremes.

When the equation $(p+q)/(p-q)\cos 2\theta = [4((1/E) - (\mu'^2/E'))/((1+\mu)/E)] - 6$ is set up, $r_{\text{extreme}} < a$. The sensitivity at the cave wall reached a maximum according to the actual situation of the project.

4. Engineering Example

4.1. Computational Models. The model adopts a circular tunnel. The calculation area of the model is 50 m × 50 m, and the mesh of the computational model is illustrated in Figure 2. The transversely isotropic plane is *xoz*. The left and right of the model are limited in the horizontal direction, and the bottom of the model is limited in the vertical direction. The initial stress distribution is illustrated in Figure 1.

The parameters of the circular tunnel are shown as follows: $a = 2.0$ m, $E = 1.0$ GPa, $E' = 0.8$ GPa, $\mu = 0.25$, and $\mu' = 0.3$. Arrangement for measuring points in the circular tunnel is shown in Figure 3. Four kinds of crustal stress parameters are illustrated in Table 1.

4.2. The First Stress Condition

(1) Sensitivity analysis of displacement to the angle

The first stress condition is $p = 10$ MPa and $q = 20$ MPa. According to FLAC3D, the radial displacement of the circular tunnel is shown in Figure 4. The radial displacements of each survey line are illustrated in Table 2.

Depending on Figure 4 and Table 2, the maximum radial displacement of each measured line appears at the wall. With the increase of the depth of the measuring point, the radial displacement decreases. For the same depth in different lines, the radial displacement decreases with the increase of the angle. The maximum radial displacement occurs in the direction of the larger initial stress, and the smallest radial displacement becomes visible in the direction of the smaller initial stress. This is in agreement with the theoretical analysis in Section 3.1.

(2) Sensitivity analysis of displacement to the radius

According to Equation (14), the following equation can be obtained by substituting known parameters:

$$\left[4\frac{(1/E) - \left(\mu'^2/E'\right)}{(1+\mu)/E}\right] - 6 = -3.16. \tag{16}$$

Then, the extreme values of different lines will be found, and the position of the maximum sensitivity is established according to the conclusion obtained in Section 3.2. Table 3 presents the sensitivity of the displacement of the radius. Table 3 shows that qualified survey lines are L1, L2, and L3. According to Equation (15), the maximum sensitivity of the displacement of the survey lines L2 and L3 to the radius appears at the cave wall. It shows that the measuring points should be arranged at the cave wall. The maximum sensitivity of the displacement of the survey line L1 to the radius appears at r_{extreme}. It shows that the measuring points should be arranged there. This is in agreement with the theoretical analysis in Section 3.2.

4.3. The Second Stress Condition. The second stress condition is $p = 5$ MPa and $q = 10$ MPa. According to FLAC3D, the radial and tangential displacements of each survey line are shown in Table 4. Comparing Tables 4 and 2, the radial displacement and tangential displacement under the two stress conditions have a multiple relationship, while the deformation law remains the same. The sensitivity analysis

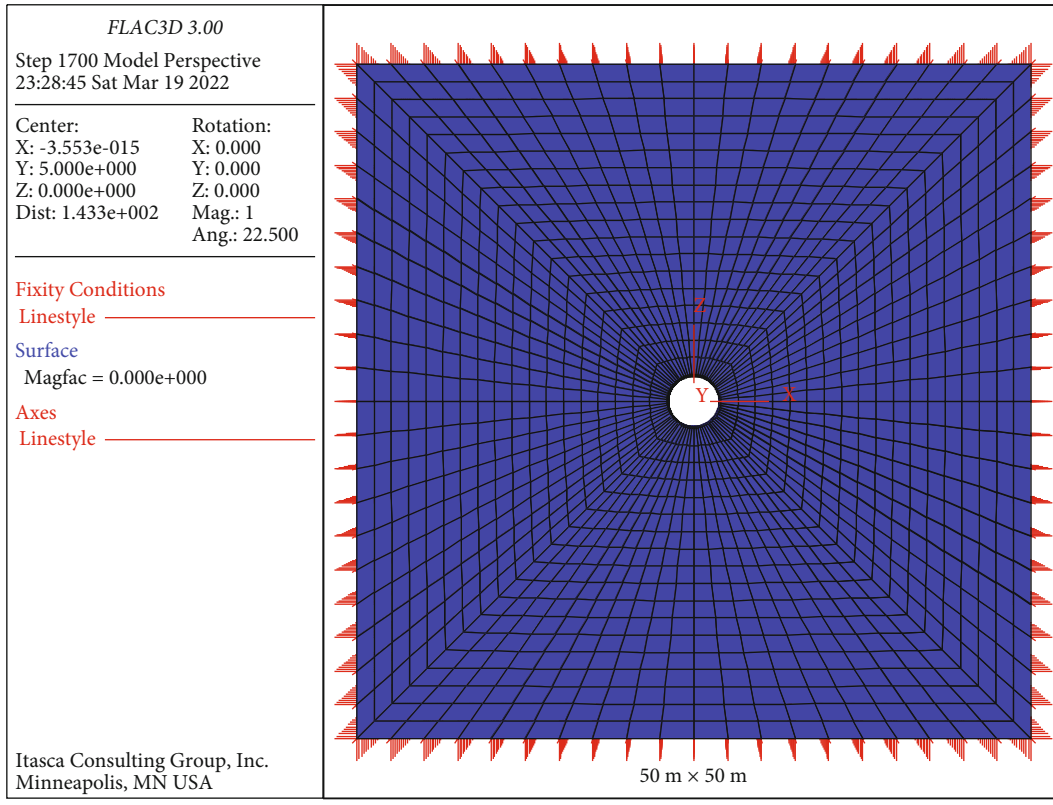

Figure 2: The mesh of the computational model.

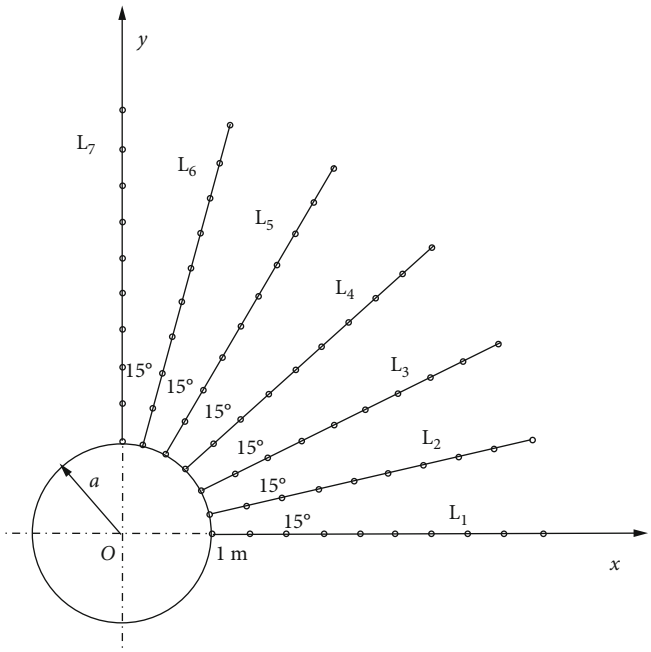

Figure 3: Arrangement for measuring points.

Table 1: Four kinds of crustal stress parameters.

Case	p (MPa)	q (MPa)
Case 1	10	20
Case 2	5	10
Case 3	20	10
Case 4	10	30

of displacement to radius is exactly the same as that of the first stress case. This confirms that as long as p/q is constant, the sensitivity of the displacement to the radius will not change with the initial ground stress.

4.4. The Third Stress Condition

(1) Sensitivity analysis of displacement to the angle

The third stress condition is $p = 20$ MPa and $q = 10$ MPa. According to FLAC3D, the radial displacement of the circular tunnel is shown in Figure 5. The radial displacements of each survey line are shown in Table 5 .

According to Figure 5 and Table 5, the maximum radial displacement of each measured line still appears at the wall though the initial geostress changes. With the increase of the depth of the measuring point, the radial displacement decreases [28–35]. For the same depth in different lines, the radial displacement increases with the increase of the angle from 0° to 90°. The maximum radial displacement occurs in

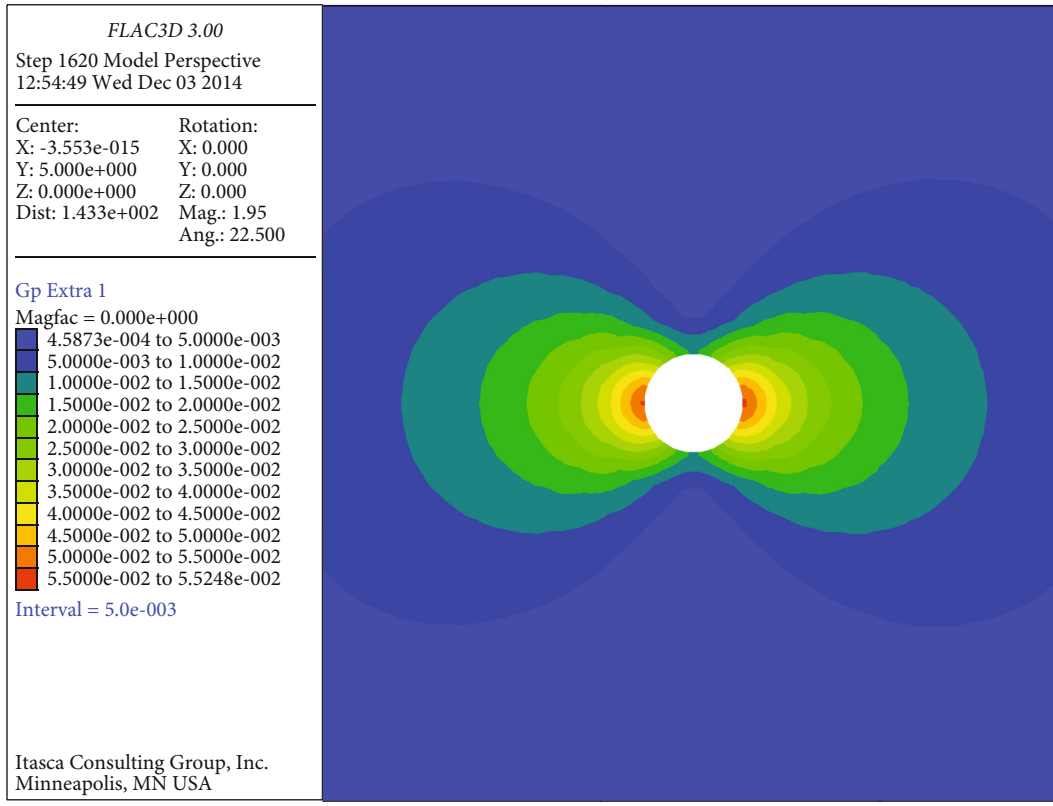

Figure 4: The radial displacement.

Table 2: The radial displacements of each survey line.

Line	L1 (cm)	L2 (cm)	L3 (cm)	L4 (cm)	L5 (cm)	L6 (cm)	L7 (cm)
N1	5.24	5.29	4.40	3.52	2.63	1.70	1.46
N2	3.84	3.56	2.88	2.06	1.13	0.65	0.45
N3	2.83	3.56	2.61	1.79	1.31	0.65	0.24
N4	2.83	2.57	1.99	1.36	0.78	0.41	0.24
N5	2.19	1.97	1.49	1.19	0.59	0.31	0.16
N6	1.76	1.57	1.49	1.01	0.59	0.24	0.13
N7	1.45	1.57	1.17	0.87	0.47	0.24	0.11
N8	1.45	1.29	0.94	0.68	0.39	0.20	0.11
N9	1.21	1.07	0.94	0.68	0.39	0.17	0.09
N10	1.03	0.90	0.78	0.54	0.32	0.15	0.08

the direction of the larger initial stress, and the smallest radial displacement appears in the direction of the smaller initial stress. This is consistent with the theoretical analysis in Section 3.1.

(2) Sensitivity analysis of displacement to the radius

Table 6 presents the sensitivity of the displacement to the radius. It shows that the qualified survey lines are L5, L6, and L7. According to Equation (15), the measuring points on the survey lines L5 and L6 should be arranged at the cave wall. The measuring points on the survey line L7 should be arranged at $r_{extreme}$. This is in agreement with the theoretical analysis in Section 3.2.

4.5. The Fourth Stress Condition

(1) Sensitivity analysis of displacement to the angle

The fourth stress condition is $p = 10$ MPa and $q = 30$ MPa. According to FLAC3D, the radial displacement of the circular tunnel is shown in Figure 6. The radial displacements of each survey line are shown in Table 7.

Table 3: The sensitivity of the displacement to the radius.

Line	θ (°)	2θ (°)	cos 2θ (°)	$p+q/(p-q)\cos 2\theta$	Judgment	$r_{extreme}$	Conclusion
L1	0	0	1	-3	>-3.16	2.03	$r_{extreme}$
L2	15	30	0.866	-3.464	<-3.16	1.95	Cave wall
L3	30	60	0.5	-6	<-3.16	1.65	Cave wall
L4	45	90	0	∞	>-3.16	Unrealistic	Fail
L5	60	120	-0.5	6	>-3.16	Unrealistic	Fail
L6	75	150	-0.866	3.464	>-3.16	Unrealistic	Fail
L7	90	180	-1	3	>-3.16	Unrealistic	Fail

Table 4: The radial displacements of each survey line.

Line	L1 (cm)	L2 (cm)	L3 (cm)	L4 (cm)	L5 (cm)	L6 (cm)	L7 (cm)
N1	2.76	2.65	2.20	1.76	1.32	0.85	0.73
N2	1.92	1.78	1.44	1.03	0.56	0.33	0.22
N3	1.41	1.78	1.31	0.89	0.65	0.33	0.12
N4	1.41	1.29	0.99	0.68	0.39	0.20	0.12
N5	1.10	0.99	0.74	0.59	0.30	0.15	0.082
N6	0.88	0.79	0.74	0.50	0.30	0.12	0.064
N7	0.73	0.79	0.58	0.44	0.24	0.12	0.053
N8	0.73	0.64	0.47	0.33	0.19	0.10	0.053
N9	0.61	0.54	0.47	0.33	0.19	0.087	0.045
N10	0.51	0.45	0.39	0.27	0.16	0.075	0.040

According to Figure 6 and Table 7, changing the initial geostress, the maximum radial displacement of each measured line still appears at the wall. And the maximum radial displacement occurs in the direction of the larger initial stress, and the smallest radial displacement appears in the direction of the smaller initial stress. This is consistent with the theoretical analysis in Section 3.1.

(2) Sensitivity analysis of displacement to the radius

Table 8 presents the sensitivity of the displacement to the radius. It shows that the qualified survey lines are L1, L2, L3, L6, and L7. According to Equation (15), the measuring points on the survey lines L3 should be arranged at the cave wall. The measuring points on the survey lines L1, L2, L6, and L7 should be arranged at $r_{extreme}$. This is in agreement with the theoretical analysis in Section 3.2.

When the stress in the vertical direction constant is kept constant and the stress in the horizontal direction increases, except for the measuring line L5, the other measuring lines will gradually have extreme points as the angle increases and the value is increasing, while the sensitivity coefficient is at the extreme point to get the maximum value. Moreover, in the larger principal stress direction, the extreme point is near the cave wall, while in the smaller principal stress direction, the extreme point is far from the cave wall. However, as the displacement gradually decreases, a larger relative error would occur. Considering the effect of error transmission, it is recommended that the measuring point is arranged near the extreme point in the direction of the larger principal stress.

5. Discussion

Based on the maximum sensitivity criterion, the problem of the optimal layout of measuring points for back analysis of displacements in transversely isotropic rock masses is investigated to determine the most suitable location for measuring points in this work. The connection between the sensitivity of displacement to the angle and radius is obtained.

Both Zhang [21] and this work are aimed at optimizing the arrangement of measuring points of the transversely isotropic rock mass. However, the work of Zhang [21] was based on the principle of maximum displacement. Three aspects are discussed as follows. Firstly, both works just analyzed the circular tunnels. Then, Zhang [21] suggested that the most suitable location for measuring points was at the cave wall or extreme value, which is consistent with the conclusion of this work. Zhang [21] mainly considered the relationship of the lateral pressure coefficient. However, in this paper, it makes further judgments according to the size relationship by Equation (15) as needed. Finally, Zhang [21] believed that the direction of the larger principal stress and the adjacent direction were suitable directions to arrange the measurement line. Similarly, in this paper, the measuring point was arranged in the area of the larger principal stress near the extreme point.

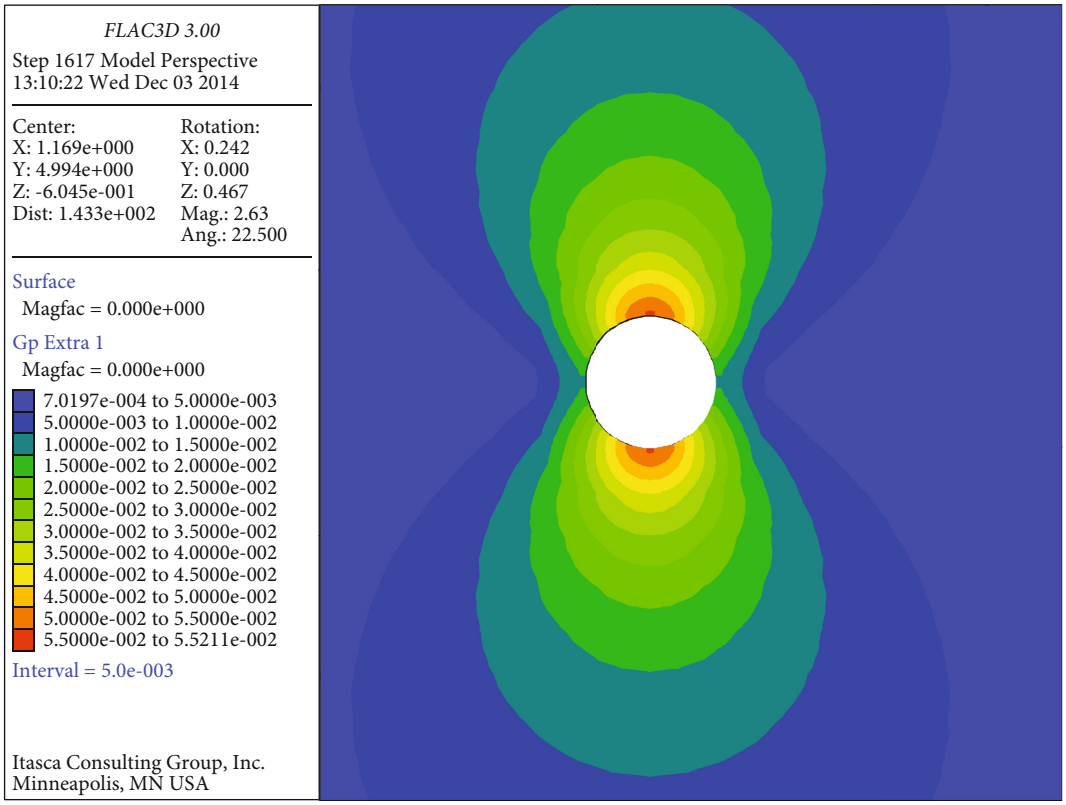

Figure 5: The radial displacement.

Table 5: The radial displacements of each survey line.

Line	L1 (cm)	L2 (cm)	L3 (cm)	L4 (cm)	L5 (cm)	L6 (cm)	L7 (cm)
N1	1.46	1.70	2.63	3.52	4.40	5.29	5.52
N2	0.45	0.65	1.13	2.06	2.88	3.56	3.84
N3	0.24	0.65	1.31	1.79	2.61	3.56	2.83
N4	0.24	0.41	0.78	1.36	1.99	2.57	2.83
N5	0.16	0.31	0.59	1.19	1.49	1.97	2.19
N6	0.13	0.24	0.59	1.01	1.49	1.54	1.76
N7	0.11	0.24	0.47	0.87	1.17	1.54	1.45
N8	0.11	0.20	0.39	0.68	0.94	1.29	1.45
N9	0.091	0.17	0.39	0.68	0.94	1.07	1.22
N10	0.079	0.15	0.32	0.54	0.78	0.90	1.03

Table 6: The sensitivity of the displacement to the radius.

Line	θ (°)	2θ(°)	cos 2θ(°)	$p+q/(p-q)\cos 2\theta$	Judgment	$r_{extreme}$	Conclusion
L1	0	0	1	3	>-3.16	Unrealistic	Fail
L2	15	30	0.866	3.464	>-3.16	Unrealistic	Fail
L3	30	60	0.5	6	>-3.16	Unrealistic	Fail
L4	45	90	0	∞	>-3.16	Unrealistic	Fail
L5	60	120	-0.5	-6	<-3.16	1.65	Cave wall
L6	75	150	-0.866	-3.464	<-3.16	1.95	Cave wall
L7	90	180	-1	-3	>-3.16	2.03	$r_{extreme}$

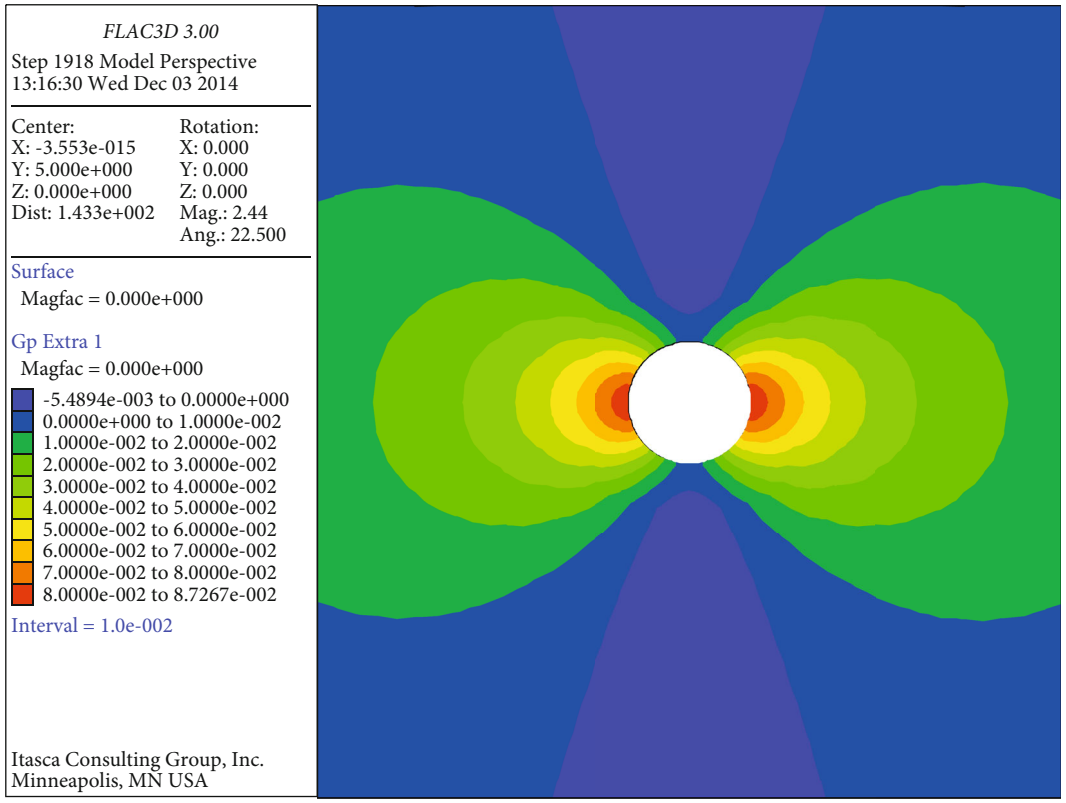

Figure 6: The radial displacement.

Table 7: The radial displacements of each survey line.

Line	L1 (cm)	L2 (cm)	L3 (cm)	L4 (cm)	L5 (cm)	L6 (cm)	L7 (cm)
N1	8.73	8.26	6.45	4.69	2.92	1.07	5.86*e*-1
N2	6.25	5.73	4.43	2.89	9.21*e*-1	-1.06*e*-1	-5.39*e*-1
N3	4.63	5.73	3.92	2.39	1.31*e*-1	-1.06*e*-1	-5.49*e*-1
N4	4.63	4.16	3.05	1.90	6.34*e*-1	-1.79*e*-1	-5.49*e*-1
N5	3.60	3.19	2.28	1.59	4.90*e*-1	-1.51*e*-1	-4.59*e*-1
N6	2.90	2.55	2.28	1.40	4.90*e*-1	-1.19*e*-1	-3.79*e*-1
N7	2.39	2.55	1.79	1.17	3.96*e*-1	-1.19*e*-1	-3.09*e*-1
N8	2.39	2.09	1.45	9.02*e*-1	3.31*e*-1	-9.21*e*-2	-3.09*e*-1
N9	2.00	1.74	1.45	9.02*e*-1	3.31*e*-1	-7.08*e*-2	-2.56*e*-1
N10	1.69	1.46	1.19	7.18*e*-1	2.81*e*-1	-5.36*e*-2	-2.13*e*-1

Table 8: The sensitivity of the displacement to the radius.

Line	θ (°)	2θ(°)	cos 2θ(°)	$p+q/(p-q)\cos 2\theta$	Judgment	$r_{extreme}$	Conclusion
L1	0	0	1	-2	>-3.16	2.23	$r_{extreme}$
L2	15	30	0.866	-2.309	>-3.16	2.16	$r_{extreme}$
L3	30	60	0.5	-4	<-3.16	1.87	Cave wall
L4	45	90	0	∞	>-3.16	Unrealistic	Fail
L5	60	120	-0.5	4	>-3.16	Unrealistic	Fail
L6	75	150	-0.866	2.309	>-3.16	6.72	$r_{extreme}$
L7	90	180	-1	2	>-3.16	5.35	$r_{extreme}$

She [23] carried out an optimized arrangement of measuring points for circular tunnels based on the principle of maximum sensitivity. She [23] selected the isotropic rock masses as the study object; in contrast, this research selected the transverse isotropic rock mass. Then, both articles obtained the sensitivity coefficients of the two principal stresses. However, She [23] limited the measuring point to the two N1 points of measuring line 1 and measuring line 7 in Figure 3 and connected the two points to get the direction of the arrangement of the measuring line. In this work, the sensitivity analysis of the radius was comprehensively analyzed, and the optimal measuring point at the extreme value instead of the cave wall was selected.

6. Conclusions

(1) The sensitivity criterion for the arrangement of measuring points in circular roadway of transversely isotropic rock mass is deduced. The sensitivity of the radius and angle of the measuring point arrangement provides the basis for the formulation of the monitoring program

(2) From the sensitivity analysis of displacement to angle, the arrangement of measuring points in the two principal stress directions is the most suitable for the inversion of parameters. At the same time, the two principal stress directions are also the priority positions in the layout scheme of measuring points

(3) According to the sensitivity of the displacement to the radius, whether the location of the most suitable measuring point is at the cave wall or the extreme value depends on the relationship between the radius and the extreme value. Further discussion is required based on the discriminants derived in this paper

(4) By changing the magnitude and direction of the principal stress, the correctness of the theoretical derivation is verified by numerical simulation, and a comprehensive analysis is carried out. The results show that the most suitable location for arranging the survey line is the area close to the extreme point in the direction of the larger principal stress

Data Availability

The data reported in this article are available from the corresponding author upon request.

Conflicts of Interest

The authors declare no conflicts of interest.

Authors' Contributions

The manuscript is approved by all authors for publication

Acknowledgments

This research is supported by the Natural Science Foundation of Henan Province (No. 222300420596) and the Joint Fund for Fostering Talents of National Natural Science Foundation of China and Henan Province (No. U1204509).

References

[1] H. Wu, G. Y. Zhao, and S. W. Ma, "Failure behavior of horseshoe-shaped tunnel in hard rock under high stress: phenomenon and mechanisms," *Transactions of Nonferrous Metals Society of China*, vol. 32, no. 2, pp. 639–656, 2022.

[2] L. Cheng, J. F. Liu, L. C. Ren Yi, and Y. L. Liao, "Study on very long-term creep tests and nonlinear creep-damage constitutive model of salt rock," *International Journal of Rock Mechanics and Mining Sciences*, vol. 146, article 104873, 2021.

[3] J. Xu, E. Wang, and R. Zhou, "Real-time measuring and warning of surrounding rock dynamic deformation and failure in deep roadway based on machine vision method," *Measurement*, vol. 149, article 107028, 2020.

[4] B. Wang, F. Dang, W. Chao, Y. Miao, J. Li, and F. Chen, "Surrounding rock deformation and stress evolution in pre-driven longwall recovery rooms at the end of mining stage," *International Journal of Coal Science & Technology*, vol. 6, no. 4, pp. 536–546, 2019.

[5] D. J. Pan, K. R. Hong, H. L. Fu, J. Zhou, N. Zhang, and G. Lu, "Influence characteristics and mechanism of fragmental size of broken coal mass on the injection regularity of silica sol grouting," *Construction and Building Materials*, vol. 269, article 121251, 2021.

[6] D. J. Pan, K. R. Hong, H. L. Fu, J. Zhou, and N. Zhang, "Experimental study of the mechanism of grouting colloidal nanosilica in over-broken coal mass," *Quarterly Journal of Engineering Geology and Hydrogeology*, vol. 54, no. 4, 2021.

[7] L. D. Yang, M. Peng, and X. F. Ma, "Optimization of the displacement measuring in surrounding rock," *Journal of Tong Ji University*, vol. 23, no. 2, pp. 129–133, 1995.

[8] Z. Y. Song and J. J. Li, "Sensitivity analysis and a new inverse algorithm of elastic parameters for gravity dam," *Journal of Sichuan University (Engineering Science Edition)*, vol. 38, no. 4, pp. 34–38, 2006.

[9] L. J. Wardle and C. M. Gerrard, "The "equivalent" anisotropic properties of layered rock and soil masses," *Rock Mechanics*, vol. 4, no. 3, pp. 155–175, 1972.

[10] W. W.-G. Yeh, "Review of parameter identification procedures in groundwater hydrology: the inverse problem," *Water Resources*, vol. 22, no. 2, pp. 95–108, 1986.

[11] M. M. Mejias, H. R. B. Orlande, and M. N. Ozisik, "Effects of the heating process and body dimensions on the estimation of the thermal conductivity components of orthotropic solids," *Inverse Problems in Engineering*, vol. 11, no. 1, pp. 75–89, 2003.

[12] J. P. Kernevez, C. Knopf-Lenoir, G. Touzot, and G. Verchery, "An identification method applied to an orthotropic plate bending experiment," *International Journal for Numerical Methods in Engineering*, vol. 12, no. 1, pp. 129–139, 1978.

[13] J. Sun, S. P. Jiang, and Y. Yuan, *Stochastic Theory and Method of Inversion Problems in Rock Mechanics*, Shantou University Press, 1996.

[14] X. Z. Yang, "Sensitive displacement component analysis and optimal placement of parametric displacement back analysis,"

Journal of Southern Institute of Metallurgy, vol. 15, no. 4, pp. 227–237, 1994.

[15] Z. H. Xiang, *Studies on rock and soil parameter identification based on displacement measurements*, Tsinghua University, Department of Engineering Mechanics, Beijing, 2002.

[16] Z. H. Xiang, G. Swoboda, and Z. Z. Cen, "Optimal layout of displacement measurements for parameter identification process in geomechanics," *International Journal of Geomechanics*, vol. 3, no. 2, pp. 205–216, 2003.

[17] Z. H. Xiang, G. Svvubuda, and Z. Z. Cen, "Parameter idenliualiun and its application in tunneling," in *Numerical Simulation in Tunneling*, G. Beer, Ed., pp. 161–200, Springer-Verlag, Wien, 2003.

[18] L. X. Huang, *Parameter identification for two-dimensional orthotropic material bodies by the boundary element method*, Tsinghua University, Beijing, 2005.

[19] L. X. Huang, "Algorithm and software design of material parameter identification for plane orthotropic material bodies," *Fiber Reinforced Plastics/Composites*, vol. 5, pp. 35–39, 2010.

[20] S. B. Li, X. J. Zhou, Y. Y. Liu, L. X. Huang, and X. W. Guo, "Algorithm and software design of material parameter identification for orthotropic composite structure based on ABAQUS," *Journal of Guilin University of Technology*, vol. 30, no. 1, pp. 159–163, 2010.

[21] Z. Z. Zhang, *Theory and application research on displacement back analysis of transversely isotropic rock mass*, Tsinghua University, Beijing, 2010.

[22] Z. Z. Zhang, Y. T. Li, W. L. Yang, S. C. Wu, X. L. Liu, and B. Zhang, "Optimization of measuring points layout around a tunnel in the transversely isotropic rock mass," *Shock and Vibration*, vol. 2021, 10 pages, 2021.

[23] Y. G. She, "Principles of optimal measured arrangement and its application for back-analysis in underground engineering," *Journal of China Coal Society*, vol. 36, no. 2, pp. 308–314, 2011.

[24] Y. G. She and C. W. Shen, "Discussion of identifiability and optimal measured arrangement for elastic back-analysis of parameters in underground tunnel engineering," *Rock and Soil Mechanics*, vol. 31, no. 11, pp. 3604–3612, 2010.

[25] Y. G. She and M. S. Wang, "Intelligent back analysis method for underground engineering interval based on optimized layout of measuring points," *China Civil Engineering Journal*, vol. S1, pp. 331–335, 2015.

[26] J. Z. Zhang, H. W. Huang, D. M. Zhang, M. L. Zhou, C. Tang, and D. J. Liu, "Effect of ground surface surcharge on deformational performance of tunnel in spatially variable soil," *Computers and Geotechnics*, vol. 136, article 104229, 2021.

[27] J. Z. Zhang, K. K. Phoon, D. M. Zhang, H. W. Huang, and C. Tang, "Novel approach to estimate vertical scale of fluctuation based on CPT data using convolutional neural networks," *Engineering Geology*, vol. 294, article 106342, 2021.

[28] W. Zhong, J. Ouyang, D. Yang, X. Wang, Z. Guo, and H. Kaijian, "Effect of the in situ leaching solution of ion-absorbed rare earth on the mechanical behavior of basement rock," *Journal of Rock Mechanics and Geotechnical Engineering*, vol. 14, 2021.

[29] Y. Guansheng Han, R. L. Zhou, Q. Tang, X. Wang, and L. Song, "Influence of surface roughness on shear behaviors of rock joints under constant normal load and stiffness boundary conditions," *Natural Hazards*, vol. 112, no. 1, pp. 367–385, 2022.

[30] X. L. Li, Z. Y. Cao, and Y. L. Xu, "Characteristics and trends of coal mine safety development," *Energy Sources, Part A: Recovery, Utilization, and Environmental Effects*, pp. 1–19, 2020.

[31] S. M. Liu, X. L. Li, D. K. Wang, and D. Zhang, "Investigations on the mechanism of the microstructural evolution of different coal ranks under liquid nitrogen cold soaking," *Energy Sources, Part A: Recovery, Utilization, and Environmental Effects*, pp. 1–17, 2020.

[32] X. L. Li, S. J. Chen, Q. M. Zhang, X. Gao, and F. Feng, "Research on theory, simulation and measurement of stress behavior under regenerated roof condition," *Geomechanics and Engineering*, vol. 26, no. 1, pp. 49–61, 2021.

[33] X. L. Li, S. J. Chen, S. M. Liu, and Z. H. Li, "AE waveform characteristics of rock mass under uniaxial loading based on Hilbert-Huang transform," *Journal of Central South University*, vol. 28, no. 6, pp. 1843–1856, 2021.

[34] X. G. Kong, D. He, X. F. Liu et al., "Strain characteristics and energy dissipation laws of gas-bearing coal during impact fracture process," *Energy*, vol. 242, article 123028, 2022.

[35] Y. Niu, E. Wang, Z. Li et al., "Identification of coal and gas outburst-hazardous zones by electric potential inversion during mining process in deep coal seam," *Rock Mechanics and Rock Engineering*, 2022.